

Ab-initio Many Body Perturbation Theory calculations of the electronic and optical properties of cyclometalated Ir(III) complexes

Marco Cazzaniga,^{†,‡} Fausto Cargnoni,^{*,†} Marta Penconi,[†] Alberto Bossi,^{*,†} and
Davide Ceresoli^{*,†}

[†]*Consiglio Nazionale delle Ricerche, Istituto di Scienze e Tecnologie Chimiche
(CNR-SCITEC), 20133 Milano, Italy*

[‡]*Present address: Department of Chemistry, University of Milan, via Golgi 19, 20133
Milano, Italy*

E-mail: fausto.cargnoni@cnr.it; alberto.bossi@cnr.it; davide.ceresoli@cnr.it

Abstract

Cyclometalated Ir(III) compounds are the preferred choice as organic emitters in Organic Light Emitting Diodes. In practice, the presence of the transition metals surrounded by carefully designed ligands allows the fine tuning of the emission frequency as well as a good efficiency of the device. To support the development of new compounds the experimental measurements are generally compared with ab-initio calculation of the absorption and emission spectra. The standard approach for these calculations is TDDFT with hybrid exchange and correlation functional like the B3LYP. Due to the size of these compounds the application of more complex quantum chemistry approaches can be challenging. In this work we used Many Body Perturbation Theory approaches (in particular the GW approximation with the Bethe-Salpeter equation)

implemented in gaussian basis sets, to calculate the quasiparticle properties and the adsorption spectra of six cyclometalated Ir(III) complexes going behind TDDFT. In the presented results we compared standard TDDFT simulation with BSE calculations performed on top on perturbative G_0W_0 and accounting for eigenvalue self consistency. Moreover, in order to investigate in detail the effect of the DFT starting point, we concentrate on Ir(ppy)₃ performing GW-BSE simulations starting from different DFT exchange and correlation potentials.

1 Introduction

Phosphorescent Organic Light Emitting Diodes (phOLEDs) are nowadays widely employed in a large number of devices, like portable light sources and displays. A huge research effort is devoted in designing new emitters with improved efficiency and operational stability.¹⁻⁶

Cyclometalated Ir(III) complexes are the preferred emitters molecules in these devices, because of their large quantum efficiency approaching unity. The large Spin Orbit Coupling (SOC) of Iridium is responsible for an efficient phosphorescent emission and the low-lying electronic transitions display a mixed Ligand-Center Metal-to-Ligand-Charge-Transfer (LC-MLCT) character. By tailoring the chemical nature of the ligands, it is possible to tune the emission frequency from the near infrared (NIR) to deep blue. Additionally, replacing one ligand in homoleptic compounds with a different one (giving rise to heteroleptic complexes) can improve the emitter performance, increase the stability of the devices, and finely tune the emission frequency in order to achieve the desired “color”.^{7,8}

To design new emitters *in-silico*, theory and computations are required to understand and predict the measured photo-physical properties of cyclometalated complexes. The standard theoretical approach for this kind of investigation is Density Functional Theory (DFT) together with its Time Dependent extension (TDDFT). Hybrid functionals (typically B3LYP, PBE0), long-range corrected hybrids (i.e. LC-PBE,⁹ LC ω -PBE¹⁰) and range-separated hybrids (i.e. CAM-B3LYP¹¹) are the most used to describe the optical absorption and emis-

sion spectra of these systems. As it turns out, the ground state properties as well as the TDDFT-calculated optical absorption and emission spectra, result in with a good agreement with experiments.^{12,13}

Anyway, the aforementioned good performances of DFT/TDDFT with hybrid functionals is somehow fortuitous. Going beyond this standard approach with wavefunctions methods, is at present unfeasible because of the large number of active electrons typical of these complexes. Accordingly, only a limited number of authors tried to adopt different approaches to benchmark or improve the accuracy of theoretical predictions. Examples are the application of the DFT+Hubbard U method,¹⁴ the explicit inclusion of SOC¹⁵⁻¹⁸ and the use of multireference approaches.^{19,20}

Many Body Perturbation Theory (MBPT), particularly the GW and Bethe Salpeter Equation (BSE)²¹ methods provide an alternative theoretical framework to access both ground and excited state properties of condensed matter²²⁻²⁷ and molecular systems.²⁸⁻³² Most importantly, the BSE method appears to describe on an equal foot local and charge-transfer excitations,³³⁻³⁵ without fine tuning of the Hartee-Fock fraction or Coulomb range separation.

In this work, we apply the GW-BSE approaches to cyclometalated Ir-complexes of technological relevance in the field of organic light emitting diodes (OLEDs). These complexes are constituted of 52-61 atoms and represent a computational challenge for the aforementioned approach, both from the CPU and memory requests. Similarly to Refs.,³⁶⁻⁴² in which the various levels of approximations of GW-BSE were benchmarked on selected sets of small organic molecules, we compare our GW results obtained with different level of self-consistency and with different DFT starting points.

We consider six Ir-complexes, with absorption and emission wavelengths spanning across the entire visible spectrum, and we calculate the optical absorption spectra starting from the B3LYP orbitals, using both the perturbative G_0W_0 and the eigenvalue self-consistent G_nW_n method. Then we discuss how discuss how the quasiparticle energies and the optical

absorption of Ir(ppy)₃, chosen as reference complex, are affected by the DFT starting point. In particular, we investigate how the results change when considering a pure local functional (BLYP), two standard hybrids with different percentage of exact exchange (B3LYP and BHLYP), and a Coulomb Attenuated functional (CAM-B3LYP). The calculated optical absorption spectra are compared to experimental results obtained in our group, reported in previous papers^{6,43} and on newly synthesized complexes.

2 Theory and methods

2.1 Review of the theory

The theoretical approaches adopted for the computations discussed in the present work are based on the Many Body Perturbation Theory.^{25,44,45} Within this framework the single quasiparticle properties can be accessed through the Hedin's equations, which consist in the following set of five equations:²²

$$G(1, 2) = G_0(1, 2) + \int G_0(1, 3)\Sigma(3, 4)G(4, 2) d3d4 \quad (1)$$

$$\Gamma(1, 2; 3) = \delta(1, 2)\delta(1, 3) + \int \frac{\delta\Sigma(1, 2)}{\delta G(4, 5)}G(4, 6)G(7, 5)\Gamma(6, 7; 3)d4d5d6d7 \quad (2)$$

$$\chi(1, 2) = -i \int G(1, 3)G(4, 1)\Gamma(3, 4; 2)d3d4 \quad (3)$$

$$W(1, 2) = v_C(1, 2) + \int v_C(1, 3)\chi(3, 4)W(4, 2)d3d4 \quad (4)$$

$$\Sigma(1, 2) = i \int G(1, 3)W(4, 1)\Gamma(3, 2; 4)d3d4, \quad (5)$$

where G is the interacting Green function, G_0 the non-interacting one, v_C is the bare Coulomb potential, W is the screened interaction; χ is the polarizability, Σ is the self-energy, and Γ is the vertex function. We adopt the notation in which a coordinate as "1" stands for the set of position, time and spin variables ($\mathbf{r}_1, t_1, \sigma_1$).

A self-consistent solution of the set of equations (1)-(5) is a challenging task and a series

of approximations is applied to reduce the complexity of the problem. The most relevant is to neglect the vertex function which yields to the so called GW approximation from the aspect of Eq. 5 upon the aforementioned assumption.

Despite the neglect of the vertex function, a self-consistent solution of the GW equations remains challenging and computationally demanding. The starting point of a large part of these simplified approaches is the quasiparticle equation:

$$\left(-\frac{\nabla^2}{2} + V_{ext} + V_H\right) \Psi_i(\mathbf{r}) + \int d\mathbf{r}' \Sigma(\mathbf{r}, \mathbf{r}', E_i) \Psi_i(\mathbf{r}') = E_i \Psi_i(\mathbf{r}) \quad (6)$$

It should be noticed that Eq. 6 is a Schrödinger like equation where the self energy Σ is a complex and non Hermitian potential.

From the first applications of the GW approximation to bulk silicon^{23,46,47} a further simplified scheme has taken root. It consists in performing only a single iteration of Hedin's equations, thus obtaining the quasiparticle energies as a perturbative correction of the DFT-KS eigenvalues (we will refer to this approach as G_0W_0):

$$E_i \simeq \epsilon_i + \langle \psi_i | \Sigma(E_i) - V_{xc} | \psi_i \rangle, \quad (7)$$

where the solution for E_i can be found either by linearizing the frequency dependency of the self-energy around ϵ_i or, as for the present case, by zero finding algorithms. This approach revealed successful in providing good band gaps in bulk materials but presented the drawback of retaining a strong dependency on the underlying approximations used in determining G_0 (the V_{xc} functional of the DFT).

This is one of the arguments that motivate to go behind a mere perturbative calculation, toward self consistent GW. Anyway, even if some results are available, simplified approaches to self consistency have been proposed. In particular Faleev and coworkers introduced the so called Quasiparticle Self-Consistent GW (qsGW).^{48,49} The basic idea is to design a static and Hermitian approximation for the self-energy, whose results are close to the full GW.

Within the qsGW approach, the self-energy assumes the following expression:

$$\langle \Psi_i | \Sigma^{qsGW} | \Psi_j \rangle = \frac{1}{2} \text{Re} \langle \Psi_i | \Sigma(\epsilon_i) + \Sigma(\epsilon_j) | \Psi_j \rangle \quad (8)$$

A qsGW calculations deals with successive evaluations of the matrix elements of Eq. 8, followed by a diagonalization of the quasiparticle equation until self-consistency is reached. A further simplification of this approach consists in updating only the quasiparticle eigenvalues while keeping fixed the starting point orbitals (we will refer hereafter to this approach as $G_n W_n$).

Within MBPT neutral excitation energies can be accessed through the Bethe-Salpeter equation,²¹ which consists in the following Dyson like equation for the two-particle correlation function L:

$$L(1, 2, 3, 4) = L_0(1, 2, 3, 4) + \int L_0(1, 2, 5, 6) \left[v_C(5, 7) \delta(5, 6) \delta(7, 8) + \frac{\delta \Sigma(5, 6)}{\delta G(7, 8)} \right] L(7, 8, 3, 4) d5d6d7d8 \quad (9)$$

where L_0 is the non-interacting correlation function. Analogously to the case of Hedin's equations, in practical applications of Eq. 9 some simplifying assumptions are made: L_0 is build from the GW quasiparticle energies and the corresponding orbitals, while the kernel in Eq. 9 is obtained assuming a GW self-energy in its static ($\omega \rightarrow 0$) limit and neglecting the $\delta W / \delta G$ term. Thanks to these approximations it is possible to rewrite the BSE as an eigenvalue problem in the particle-hole space, similar to the Casida's formalism for the TDDFT:⁵⁰

$$\begin{pmatrix} A & B \\ -B^* & -A^* \end{pmatrix} \begin{pmatrix} X \\ Y \end{pmatrix} = \omega \begin{pmatrix} X \\ Y \end{pmatrix} \quad (10)$$

where the matrix A and B are respectively:

$$\begin{aligned}
A_{ia,jb} &= (E_a - E_i)\delta_{ij}\delta_{ab} - \alpha^{S/T} (ia|v_C|jb) + (ij|W|ab) \\
B_{ia,jb} &= -\alpha^{S/T} (ia|v_C|bj) + (ib|W|aj)
\end{aligned}
\tag{11}$$

where i, j are occupied state and a, b are virtual ones; $\alpha^{S/T}$ is 2 for singlet final states and 0 for triplet ones; $(ij|V|kl) = \int d\mathbf{r} \int d\mathbf{r}' \psi_i(\mathbf{r})^* \psi_j(\mathbf{r}) V(\mathbf{r}, \mathbf{r}') \psi_k(\mathbf{r}')^* \psi_l(\mathbf{r}')$ is a two-electron integral, and $W(\mathbf{r}, \mathbf{r}') = W(\mathbf{r}, \mathbf{r}', \omega \rightarrow 0)$. The diagonalization of this matrices allows to obtain the excitation energies and oscillator strengths, which are the necessary ingredients to simulate optical spectroscopies.

2.2 Basis set convergence

The basis set convergence of GW and BSE calculations has been studied and reported extensively in Refs.^{29,36,42,51,52} We first analyzed the basis set convergence of both G_0W_0 and BSE calculations, on a small set of eight organic molecules that constitute the cyclometalated complexes under study, using the B3LYP functional. The molecules are reported in Fig. 1. We used the Dunning basis set series *cc-pVnZ* and *aug-cc-pVnZ*. The G_0W_0 HOMO and LUMO are reported in Fig. 2. As shown in Fig. 2, both the HOMO and LUMO converge from above as a function of the basis set size. For this set of molecules, the augmented basis set converges faster. Our results show that the *cc-pVTZ* basis set is capable to predict HOMO and LUMO energies within ~ 0.1 eV of the largest basis set. Likewise, we report in Fig. 3 the first eight low lying excited states computed with BSE. Our results show again that the *cc-pVTZ* basis set is capable to predict the first excitations energies within ~ 0.1 eV of the most converged basis set. One notable exception is *acac* where only the first two low lying excitations are well converged with the *cc-pVTZ*. In this case, there are two excited states whose energy decreases steeply with the basis set size, and crosses with other well-converged excited states. This situation is similar to what is reported in Ref.⁵³ for the

pyrrole molecule. We note in passing that benzene, pyrrole, furane and thiophene display a problematic convergence with respect to the basis set (see Fig. S26 of the supplementary information). However, our set of molecules shows a fast convergence behavior with respect to basis set size.

Given our results and observations, we decided to employ the cc-pVTZ basis set in the subsequent calculations, as it provides a convenient trade off between accuracy and computational cost.

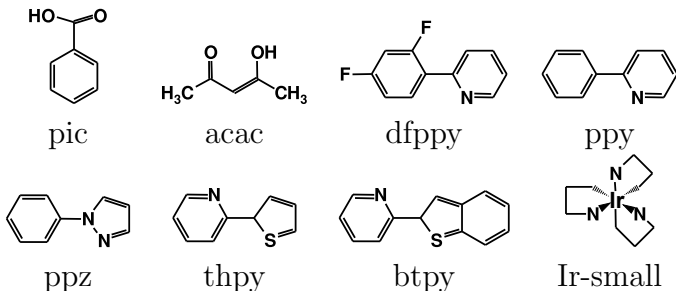


Figure 1: Set of molecules used to analyze the basis set convergence of G_0W_0 and BSE calculations. For the *acac* molecule we choose the enolic form, which is more stable than the keto form in gas phase. The *Ir-small* complex is taken from Ref.¹⁹

2.3 Computational details

Next we performed excited state simulations on six different Ir(III) cyclometalated complexes, both homoleptic and heteroleptic, which represent the standard red, green or blue OLED emitters. In particular we addressed: FIrpic, Ir(ppy)₃, Ir(ppy)₂acac, Ir(ppz)₃, Ir(thpy)₃, and Ir(btpy)₂acac, whose molecular structures are represented in Fig. 4. In the case of homoleptic compounds we considered the facial isomer, while for the heteroleptic complexes we selected the trans one, since the synthesis protocols generally produce these isomers.

Optimized geometries of the six complexes in their electronic ground state have been determined with the Gaussian09 package,⁵⁴ adopting a 6-31G(d,p) basis set for the light atoms and an aug-cc-pVDZ + ECP (Effective Core Potential) for Ir. Spin orbit coupling is not treated explicitly in our calculations, but is included through the ECP, at the scalar-

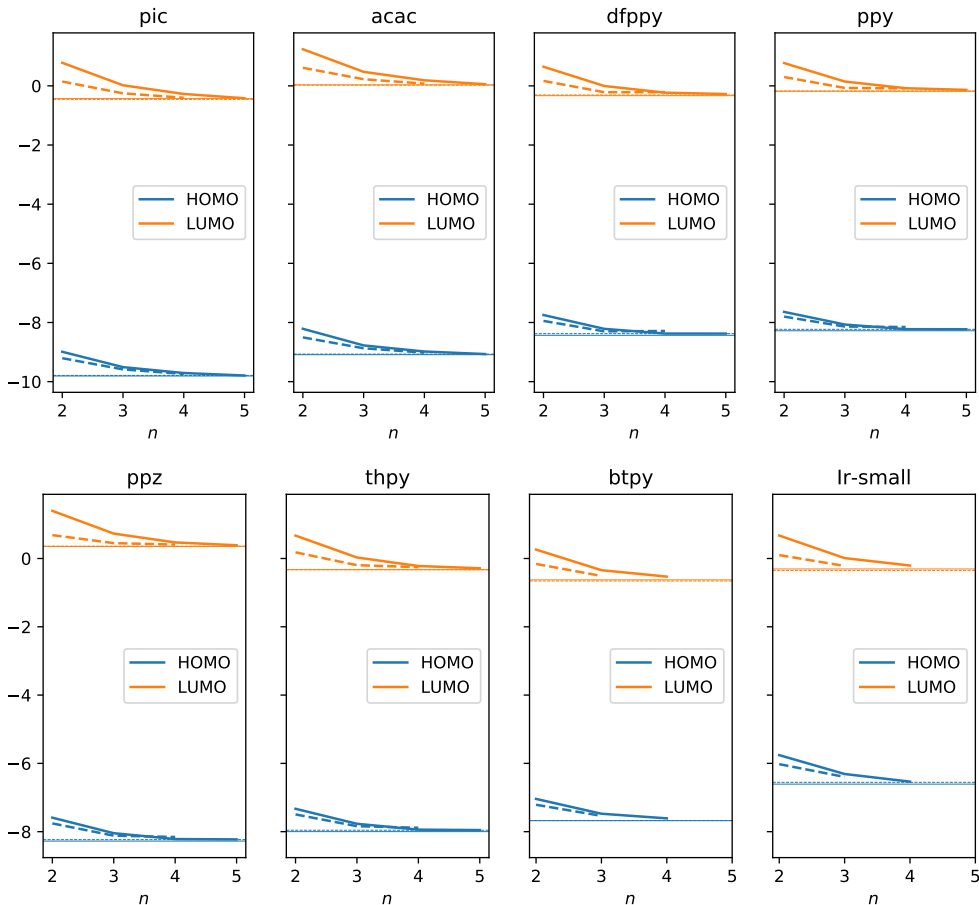


Figure 2: Calculated G_0W_0 HOMO and LUMO as a function of the basis set size. Solid thick lines: cc-pVnZ. Dashed thick lines: aug-cc-pVnZ. Thin lines: complete basis set extrapolation as $E_\infty + A/n^3$.

relativistic level. Smith and coworkers¹⁵ showed that at the TDDFT level, SO has a negligible effect on absorption spectrum, but a large impact on the magnetic circular dichroism (MCD) spectra of cyclometalated Ir(III) complexes. All computations have been carried out at the B3LYP level of theory. In the case of Ir(ppy)₃, we tested the performance of three more functionals, namely BLYP, BHLYP and CAM-B3LYP.

Excited state calculations were performed with the MolGW (version 2.A) code^{29,55} at the TDDFT, GW and BSE levels of theory, with the single exception of the TDDFT simulation of Ir(ppy)₃ with the CAM-B3LYP f_{xc} , performed with Gaussian09. We selected the cc-pVTZ basis set for all the atoms, and we adopted the Resolution of Identity (RI) for the four center integrals. Also in this case we used an ECP for describing the Ir core electrons. In all

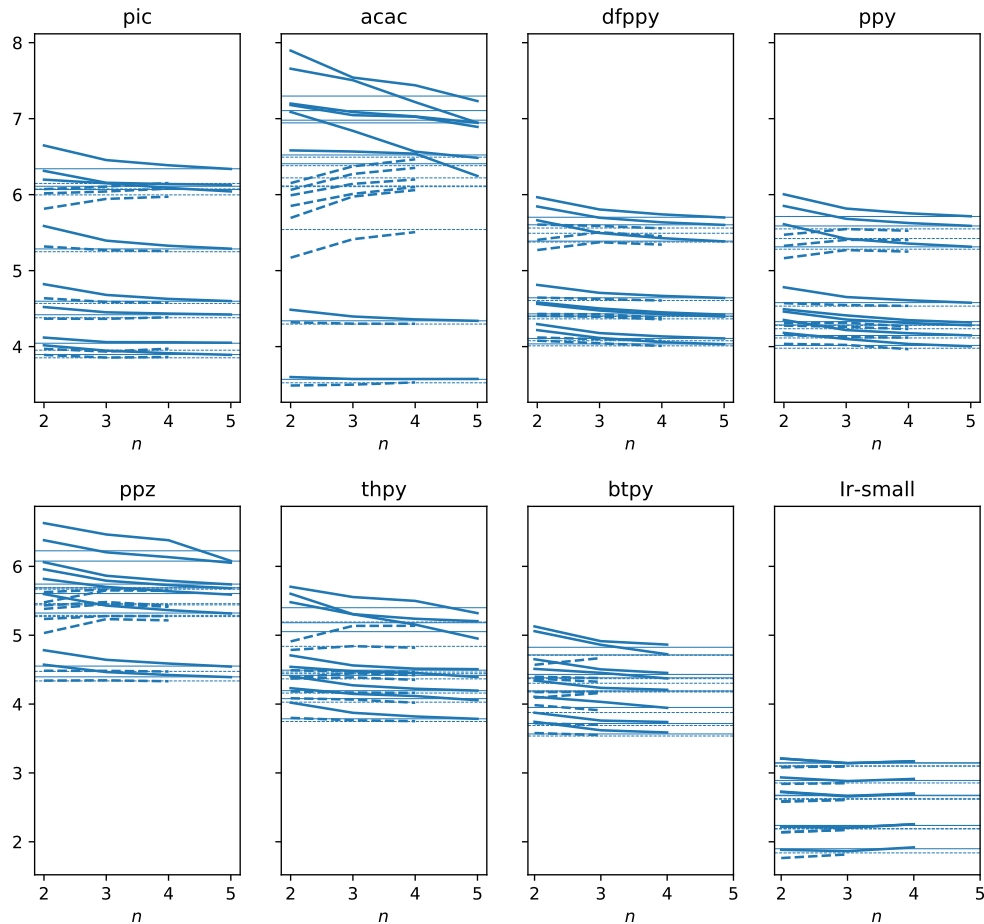
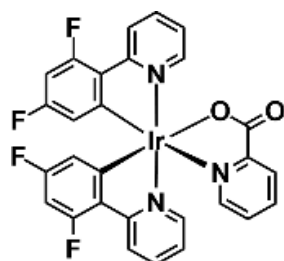


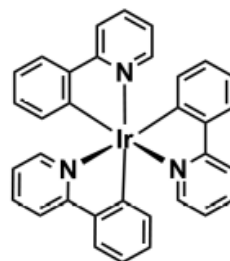
Figure 3: Calculated low lying BSE excitation energies as a function of the basis set size. Solid thick lines: cc-pVnZ. Dashed thick lines: aug-cc-pVnZ. Thin lines: complete basis set extrapolation as $E_\infty + A/n^3$.

computations we adopted the frozen core approximation. We couldn't use the aug-cc-pVTZ for the large Ir(III) complexes because it required too much memory. As we showed in Sec. 2.2, the cc-pVTZ basis set can provide converged results within ~ 0.1 eV.

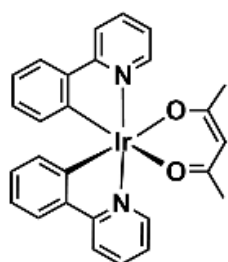
At TDDFT and BSE level we included only the lowest 500 orbitals (i.e. up to 32–40 eV depending on the molecule), which proved to ensure converged results. The eigenvalue self-consistent $G_n W_n$ calculations consisted in five iterations, and we observed that after the third iteration, eigenvalues reached self-consistency to 10^{-3} eV. We did not simulate vibrational side-bands, neither solvent effects. We broadened the absorption spectra with a 0.1 eV wide gaussian function, which yields more peaks/features than the experimental spectra.



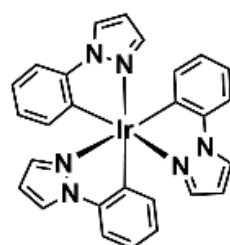
Irpic



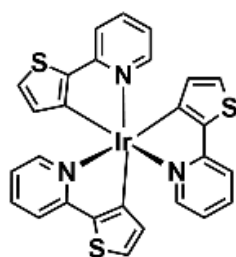
Ir(ppy)₃



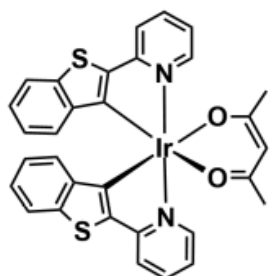
Ir(ppy)₂acac



Ir(ppz)₃



Ir(thpy)₃



Ir(btpp)₂acac

Figure 4: Scheme of the 6 complexes addressed in this work.

The most expensive part of the calculation is the GW iteration. We run our calculations on 8 cluster nodes, equipped with 2×18-core Intel Xeon E5-2697v4 CPUs and 128 Gb RAM per node. A full G_nW_n (five iterations) calculation required nearly 24 hours on this machines, and the peak memory usage reported by the code was 1.3 Gb per MPI process (288 MPI processes). Conversely, each BSE calculation required ~ 1 hour with a peak memory usage of 0.4 Gb per MPI process.

3 Experiments

Of the six cyclometalated complexes FIrpic was purchased from SigmaAldrich and used as received. The other complexes were synthesized following the procedure reported in the following papers: Ir(ppy)₃;⁵⁶ Ir(ppy)₂acac;⁵⁷ Ir(ppz)₃.⁵⁸ Ir(thpy)₃ was instead synthesized according to slight modified procedure of Ref.⁵⁹ using AgOTf instead of AgPF₆, starting from [Ir(ThPy)₂Cl]₂ (21.8% yield). The absorption spectra of FIrpic, Ir(ppy)₃ and Ir(ppy)₂acac where measuread and reported in previous works,^{6,43} whereas, for the other complexes, UV/Vis absorption spectra were obtained on Agilent 8453 spectrophotometer in 1 cm path length quartz cell with dichloromethane.

4 Quasiparticle and optical absorption of Ir(III) complexes

4.1 Quasiparticle energies

In Table 1 we reported the values of the HOMO-LUMO gaps of the complexes addressed in the present work. At the DFT-B3LYP level of theory the results are consistent with previously reported values. In particular, ordering the complexes by increasing gaps we obtain the following sequence: Ir(btpy)₂acac < Ir(ppy)₂acac < Ir(thpy)₃ < Ir(ppy)₃ < FIrpic < Ir(ppz)₃. Moving to the G_0W_0 corrected gaps we observe a large opening of the HOMO-

LUMO gaps, as expected, which is further enlarged when the self-consistency on eigenvalues is included (G_nW_n). Within these latter approaches we register a slight modification of the ordering of energy gaps, which becomes: $\text{Ir}(\text{btpy})_2\text{acac} < \text{Ir}(\text{ppy})_3 < \text{Ir}(\text{ppy})_2\text{acac} < \text{Ir}(\text{thpy})_3 < \text{FIrpic} < \text{Ir}(\text{ppz})_3$. However, we note that at these levels of theory the gaps of $\text{Ir}(\text{ppy})_3$, $\text{Ir}(\text{ppy})_2\text{acac}$ and $\text{Ir}(\text{thpy})_3$ are almost equal.

Inspecting the frontier molecular orbitals reported in Table S1–S2 of the Supplementary Information, it is possible to observe that, in agreement with the expectations for this class of compounds, the highest occupied orbitals present significant contribution coming from the central Ir, while the lowest virtual orbitals are mainly located on the ligands. In homoleptic compounds the frontier orbitals are spread over all ligands, while this is not the case in heteroleptic complexes. Indeed, in FIrpic no contribution of the HOMO is found on the ancillary ligand, while the LUMO behaves at the opposite, being mostly located on the picolate fragment. In $\text{Ir}(\text{ppy})_2\text{acac}$ and $\text{Ir}(\text{btpy})_2\text{acac}$, neither the HOMO nor the LUMO present relevant contributions on the acac moiety. Even though we didn't impose symmetry, $\text{Ir}(\text{ppy})_3$, $\text{Ir}(\text{ppz})_3$ and $\text{Ir}(\text{thpy})_3$ have C_3 symmetry whose irreps can be singly (A) or doubly degenerate (E). The presence of nearly degenerate eigenvalues is visible in Table S3. $\text{Ir}(\text{ppy})_2\text{acac}$ and $\text{Ir}(\text{btpy})_2\text{acac}$ display instead C_2 symmetry while FIrpic is C_1 . Therefore, eigenvalue degeneracies can only be accidental in these compounds.

In Fig. 5 the trend of the quasiparticle energies calculated at the DFT-B3LYP level are compared with the results obtained from the G_0W_0 and G_nW_n approximations. It is possible to notice how the opening of the HOMO-LUMO gap is coming from a decrease of the energies of occupied orbitals and a comparable increase in the energy of the virtual orbitals. Furthermore, with the exception of FIrpic, in the present series of compounds, neither the G_0W_0 nor the G_nW_n approximation modify the orbital ordering. In fact, as shown in Table S3, the quasiparticle correction to the B3LYP eigenvalues of FIrpic lead to an inversion between the LUMO and LUMO+1. As we will see later, the inversion of quasiparticle orbitals will yield the inversion in the orbitals involved in the first singlet

excitation of FIrpic.

Table 1: HOMO-LUMO gap (eV) of molecules addressed in the present work calculated as difference of DFT-KS eigenvalues compared to G_0W_0 and G_nW_n results. Calculations have been performed on top on a B3LYP DFT starting point.

		DFT-B3LYP	$G_0W_0@B3LYP$	$G_nW_n@B3LYP$
FIrpic	Present	3.614	6.066	6.673
	Ref. ⁶⁰	3.76		
	Ref. ⁸	3.73		
	Ref. ⁶¹	3.746		
Ir(ppy) ₃	Present	3.569	5.745	6.354
	Ref. ⁶²	3.565		
	Ref. ⁶¹	3.660		
Ir(ppy) ₂ acac	Present	3.449	5.763	6.361
	Ref. ⁶²	3.456		
Ir(ppz) ₃	Present	4.305	6.783	7.374
	Ref. ⁶³	4.471		
Ir(thpy) ₃	Present	3.546	5.800	6.372
Ir(btpy) ₂ acac	Present	3.119	5.334	5.857

Before moving to the discussion of excited state properties, we compute and report in Table 2 the Ionization Potential (IP) and Electron Affinities (EA) of the compounds, comparing the results with available experimental data. As already shown by Korbelt et al., ⁶⁴ we notice that the IP differences between the Δ SCF and the GW results are rather small. In detail the G_0W_0 values are slightly smaller than the Δ SCF ones, while the G_nW_n are larger. Anyway, the three approaches provide values which overestimate the available data.

The behavior of the EA is more complex. There is not a straightforward agreement of Δ SCF results against GW. This can be ascribed to the artificial stabilization of anions in DFT using a localized basis set. Unfortunately, the exiguity of available experimental data does not allow us to draw a definite conclusion about the performance of the methods, regarding the determination the EA. Note that Ir(ppz)₃ is predicted to have negative electron affinity, i.e. the anion is unstable with respect to the neutral molecule and one electron at infinity. From the experimental point of view, the Ir(ppz)₃ anion would exist as a long-lived resonance with the states of the continuum.

Table 2: Vertical ionization potential and electron affinity (eV) of the molecules addressed in the present work calculated with the Δ SCF approach compared to G_0W_0 and G_nW_n results. Calculations have been performed on top on a B3LYP starting point.

	I.P.	E.A.
	FIrpic	
Experiment ⁶⁵	5.91	
Δ SCF Ref. ⁸	6.68	0.52
Δ SCF Ref. ⁶⁰	6.69	0.50
Δ SCF	6.886	0.900
G_0W_0	6.792	0.662
G_nW_n	7.102	0.429
	Ir(ppy) ₃ fac	
Experiment ⁶⁶	5.27	1.86
Experiment ⁶⁵	5.10	
G_0W_0 Ref. ⁶²	5.94	0.08
Δ SCF	6.187	0.451
G_0W_0	6.085	0.340
G_nW_n	6.403	0.050
	Ir(ppy) ₂ acac	
G_0W_0 Ref. ⁶²	5.97	0.03
Δ SCF	6.197	0.383
G_0W_0	6.082	0.313
G_nW_n	6.385	0.011
	Ir(ppz) ₃ fac	
Experiment ⁶⁵	5.03	
Δ SCF	6.424	-0.181
G_0W_0	6.347	-0.436
G_nW_n	6.655	-0.739
	Ir(thpy) ₃ fac	
Δ SCF	6.262	0.498
G_0W_0	6.191	0.391
G_nW_n	6.480	0.108
	Ir(btpy) ₂ acac	
Δ SCF	6.031	0.682
G_0W_0	5.976	0.642
G_nW_n	6.233	0.376

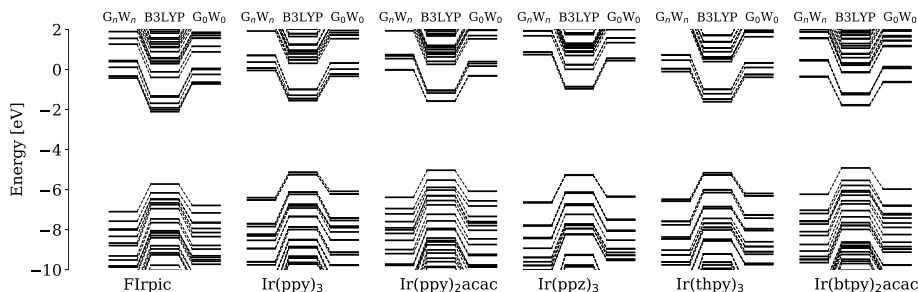


Figure 5: Quasiparticle energies of the six complexes addressed in the present work. Comparison of eigenvalues obtained from a DFT-B3LYP calculations compared to G_0W_0 and G_nW_n results obtained on top of the B3LYP ground state.

4.2 Optical absorption

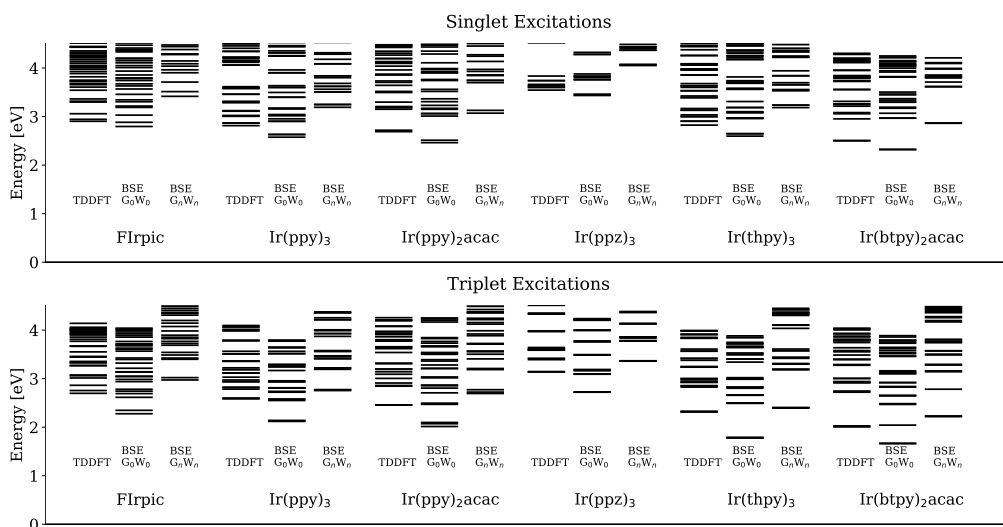


Figure 6: Lowest energy singlet and triplet excitation energies for the six complexes addressed in the present work. Calculations have been performed at the TDDFT-B3LYP level as well as from the BSE on top on G_0W_0 and G_nW_n results.

Figure 6 reports a plot of the excitation energies of the studied complexes, which are collected in Table S3–S15 of the supporting information. The general trend for both singlet and triplet excitations compared to TDDFT results is a decrease of the energies when a perturbative G_0W_0 is chosen as starting point for the BSE calculation, while we observe

the opposite behavior for results obtained on top of a G_nW_n calculation. Differences between $BSE@G_0W_0$ and $BSE@G_nW_n$ estimates of electron excitation energies are quite large, amounting to about 0.5 eV.

In more detail, in FIrpic we can observe that the four lowest singlets present essentially a single transition character. They involve transitions from HOMO-2, HOMO-1 and HOMO toward the orbitals from LUMO to LUMO+2, and present a mixed Metal to Ligand Charge Transfer (MLCT) and Ligand Centered (LC) character typical of these complexes. Comparing TDDFT and BSE results the most interesting difference is that the HOMO-LUMO excitation (which involves the picolate) corresponds to S_1 at TDDFT level, while becomes S_3 in both BSE calculations. As a matter of fact, this is due to the inversion of the LUMO and LUMO+1 in the quasiparticle calculations.

By inspecting the frontier orbitals of Table S2, we notice that in GW-BSE, the first singlet transition displays a MLCT with a larger metal contribution. The case of $Ir(ppy)_3$ is simpler. Here the lowest singlets still present a mixed MLCT-CT character and are dominated by a single transition involving the same set of orbitals of FIrpic. The differences between TDDFT and BSE results are limited to the aforementioned modification in the adsorption frequencies. Note that lowest singlets are nearly degenerate, by virtue of the C_3 symmetry. For the heteroleptic $Ir(ppy)_2acac$ the S_1 and the S_2 are still dominated by a single transition HOMO \rightarrow LUMO+1 and HOMO \rightarrow LUMO, respectively, in all the three approximations tested in this work. By consequence both these transitions are mixed MLCT and LC, with a limited contribution coming from the ancillary ligand. On the contrary, more than one transition contributes to higher singlets, yielding to nontrivial differences between the various theoretical frameworks. Singlet excitations in $Ir(ppz)_3$ and $Ir(thpy)_3$ instead behave similarly. The only excitation which does not change among the three theoretical approaches is S_1 , which is essentially a HOMO \rightarrow LUMO transition (the orbital analysis proves a mixed MLCT and LC character of S_1 also for this complex), while for the singlets immediately above the character of the transitions are comparable in the two BSE calculations but

differ from TDDFT results. In the last compound, Ir(btpy)₂acac, both S₁ and S₂ present a multiple transition character dominated by the contributions from HOMO→LUMO and HOMO→LUMO+1 (yielding to an admixture of MLCT and LC transitions at which the acac ligand contributes marginally) within all the three approaches, while the successive singlet excitations are sorted in a similar way for the BSE results but differ from the TDDFT ones.

The analysis of triplet excitations is somewhat more complex. For example, in the case of FIrpic the difference between the three approaches tested does not limit to the absolute value of the excitation energy, as mentioned at the beginning of the section. Indeed, the orbital components of the transitions are never the same comparing different methods. Much easier is the case of Ir(ppy)₃ for which, similarly to singlet excitations, the triplets presents contributions coming from the same transitions both in TDDFT and in BSE based on both the starting points. For Ir(ppy)₂acac the most significant difference is the switch of T₅, which becomes T₁ and T₃ in the BSE@G₀W₀ and BSE@G_nW_n respectively. The following two compounds addressed in the present work, Ir(ppz)₃ and Ir(thpy)₃, present an intricate behavior. Even the lowest energy triplet presents contributions originating from multiple transitions, and it is rather difficult to observe similarities between the different approaches adopted. In the last compound, Ir(btpy)₂acac, the two lowest triplets present the same character in TDDFT and in BSE calculations, while the successive ones are consistent only comparing BSE calculations based on the two different GW flavors. Finally, we compared the G_nW_n-BSE excitations of FIrpic with and without the Tamm-Dancoff Approximation (TDA), and we found that within TDA, the lowest-lying triplet energies are higher by 0.02–0.08 eV.

Figure 7 reports the comparison of calculated extinction coefficients compared with measurements. As expected, the standard TDDFT-B3LYP level of theory produces theoretical spectra in fairly good agreement with experiments, providing adsorption edges close to the experimental ones and capturing all the main features present in the measurements. The

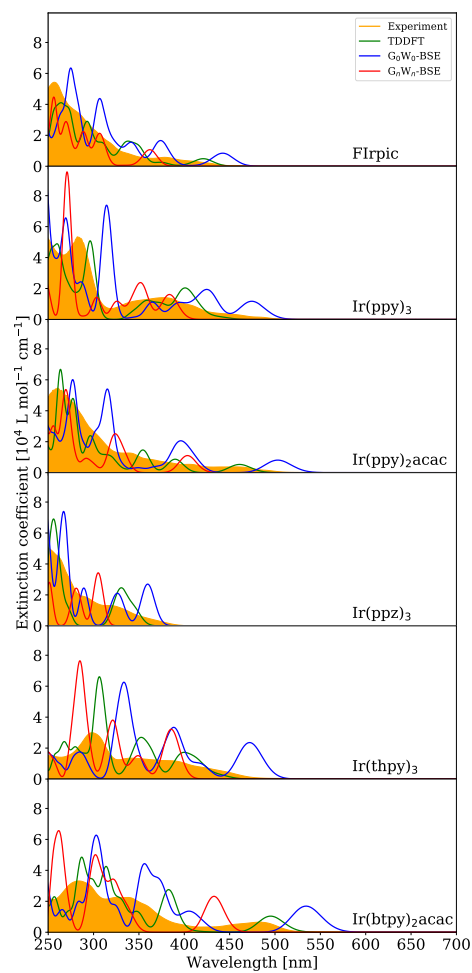


Figure 7: Extinction coefficient of the 6 complexes addressed in the present work. Calculations have been performed at the TDDFT-B3LYP level as well as from the BSE on top on G_0W_0 and G_nW_n results.

redshift of the excitation energies obtained from the BSE@G₀W₀ results yields to an overestimation of the wavelength at which these complexes starts to absorb light, as well as to a similar shift of the main features of the spectra. On the contrary, the BSE@G_nW_n extinction coefficients behave in the opposite way, presenting a blueshift of the adsorption edges and of the peaks of the spectra. To summarize, the TDDFT results provide a better agreement with experiments, with respect to the GW-BSE, starting from B3LYP molecular orbitals.

5 Functional dependence of the Ir(ppy)₃ properties

To quantify the dependence of the electronic properties of Ir complexes on the choice of the exchange-correlation functional, we focussed on Ir(ppy)₃ and compared four DFT starting points, namely a pure local functional (BLYP), two standard hybrids with different percentage of exact exchange (B3LYP and BHLYP), and a Coulomb Attenuated functional (CAM-B3LYP). A similar study on the same complexes, only at the DFT/TDDFT level, can be found in Ref.⁶⁷

5.1 Quasiparticle energies

The HOMO-LUMO gaps of Ir(ppy)₃ calculated with the different approaches used in this work are tabled in Table 3. As expected, at DFT level, the HOMO-LUMO gap increases with the increase of the percentage of exact exchange in V_{xc} , from a too much underestimated value of 2.1 eV with the pure BLYP functional to around 6 eV with the BHLYP and the CAM-B3LYP functionals. Quasiparticle energies corrected by G₀W₀ display an opening of the HOMO-LUMO gap with respect to DFT results. Even if these results are closer to each other than DFT ones, as shown in benchmark systems,^{36,37,64} they retain a significant dependence on the DFT starting point. On the contrary, when self consistency on eigenvalues is considered, the results are less sensitive to the approximation used for the DFT simulations, with HOMO-LUMO gaps ranging between 6.2 and 6.6 eV.

Table 3: HOMO-LUMO gap (eV) of $\text{Ir}(\text{ppy})_3$ calculated as difference of DFT-KS eigenvalues compared to G_0W_0 and G_nW_n results. Calculations have been performed on top on a BLYP, B3LYP, BHLYP, and CAM-B3LYP DFT starting point.

		DFT	G_0W_0	G_nW_n
BLYP	Present	2.096	5.00	6.243
B3LYP	Present	3.569	5.745	6.353
	Ref. ⁶²	3.565		
	Ref. ⁶¹	3.660		
BHLYP	Present	5.860	6.541	6.654
CAM-B3LYP	Present	6.117	6.425	6.498

To visualize the effect of the different approximations tested in this section, we plot the quasiparticle energy in Fig. 8. Also in this case the opening of the HOMO-LUMO gap arises from the decrease of the energies of the occupied states and a comparable increase of the energies of the virtual states, which is larger within G_nW_n than with G_0W_0 for all the XC functionals tested. In addition, the magnitude of the GW corrections is larger when a V_{xc} with low percentage of exact exchange is chosen as starting point.

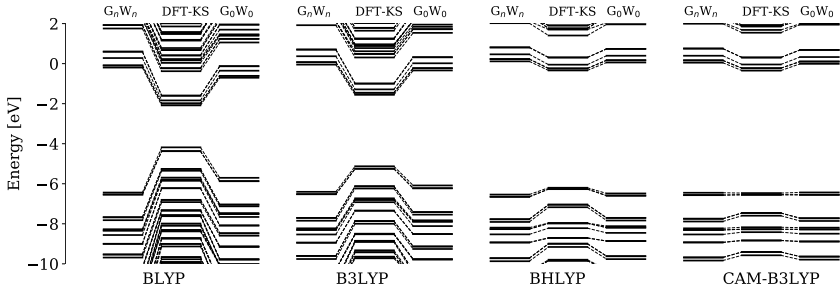


Figure 8: Quasiparticle energies of $\text{Ir}(\text{ppy})_3$ obtained as DFT-KS eigenvalues compared to G_0W_0 and G_nW_n results. Calculations have been performed on top on a BLYP, B3LYP, BHLYP, and CAM-B3LYP DFT starting point.

In Table 4 we compare our calculated quasiparticle energies against experimental measurements of the Ionization Potential (IP) and Electron Affinities (EA), as well as calculations performed with the ΔSCF method. The Ionization Potential the results obtained from the ΔSCF are rather close to both the G_0W_0 and G_nW_n values, although they all overestimate the experimental results for the Ionization Potential. A similar conclusion does not apply

straightforwardly for the Electron Affinities, where in the particular case of the CAM-B3LYP functional the Δ SCF method and the GW are in disagreement with the sign. Additionally, the disagreement with the experimental value is much worse than for IP.

Table 4: Ionization potential and electron affinity (eV) of Ir(ppy)₃ calculated with the Δ SCF approach compared to G_0W_0 and G_nW_n results. Calculations have been performed on top of a BLYP, B3LYP, BHLYP, and CAM-B3LYP DFT starting point.

	I.P.	E.A.
Experiment ⁶⁶	5.27	1.86
Experiment ⁶⁵	5.10	
BLYP		
Δ SCF	5.887	0.610
G_0W_0	5.704	0.705
G_nW_n	6.441	0.198
B3LYP		
Δ SCF	6.187	0.451
G_0W_0	6.085	0.340
G_nW_n	6.403	0.050
BHLYP		
Δ SCF	6.127	-0.142
G_0W_0	6.484	-0.057
G_nW_n	6.540	-0.114
CAM-B3LYP		
Δ SCF	6.294	0.078
G_0W_0	6.434	0.010
G_nW_n	6.451	-0.048

5.2 Optical absorption

Figure 9 represents the behavior of the excitation energies for Ir(ppy)₃ singlets and triplets calculated within TDDFT, BSE@ G_0W_0 and BSE@ G_nW_n , performed on top of DFT results obtained with four different V_{xc} . At the TDDFT level the excitation energies of both singlets and triplets increase with increasing percentage of exact exchange in the f_{xc} kernel. Similarly to quasiparticle energies, the excitation energies obtained from a BSE calculation performed on top of perturbative GW calculations, still retain a marked dependency on the DFT starting point and they are always smaller than the respective TDDFT counterparts. On the

contrary, the results obtained from the BSE on top on G_nW_n present a smaller dependence from the choice of the exchange and correlation functional, and only limited differences in the excitation energies plotted in Fig. 9 can be observed. These findings are overall consistent with previously published benchmarks.^{51,53,68} Both singlets and triplets excitation energies computed at BSE@ G_nW_n level are always located at higher energies with respect to BSE@ G_0W_0 ones. A general trend is not observed when comparing BSE and TDDFT results. Indeed, while for BLYP and B3LYP functionals the BSE@ G_nW_n excitation energies are larger than the TDDFT ones, the opposite applies in the case of BHLYP and CAM-B3LYP. Energy differences among the three approaches reduces as the percentage of exact exchange in V_{xc} increases, ranging from more than 1 eV in the BLYP case to about 0.1 eV when adopting the CAM-B3LYP functional.

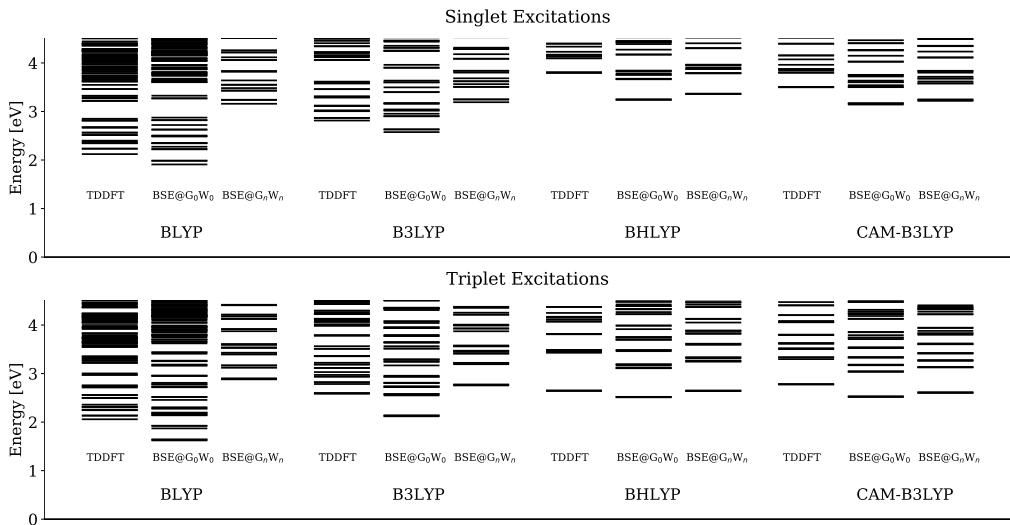


Figure 9: Lowest energy singlet and triplet excitation energies of $\text{Ir}(\text{ppy})_3$ obtained at the TDDFT level as well as from the BSE on top on G_0W_0 and G_nW_n results. Calculations have been performed on top on a BLYP, B3LYP, BHLYP, and CAM-B3LYP DFT starting point.

The character and orbital contributions to the lowest excitations are reported in Table S18-S25. In particular, the lowest singlets present a comparable character for TDDFT,

BSE@G₀W₀, and BSE@G_nW_n, when the BLYP and B3LYP functionals are used as starting point, while the comparison is less straightforward for BHLYP and CAM-B3LYP. In these last cases, but for few transitions, the character of the transitions between TDDFT and BSE result present noticeable differences, while they involve mostly the same set of orbitals in both the BSE calculations.

On the contrary, when the B3LYP functional was chosen as starting point, we did not observe differences between the TDDFT and BSE for the triplet transitions. For the other V_{XC} the character of the lowest triplet excitations remains the same between the two BSE methods but is different from TDDFT. It is worth to notice how the lowest triplet present a character different from HOMO→LUMO only for TDDFT based on a BHLYP and CAM-B3LYP functionals.

We report in Figure 10 the comparison between the experimental extinction coefficient for Ir(ppy)₃ and the ones obtained from singlet excitations (we remark that to neglect of spin-orbit coupling, as in the present study, causes transitions to triplet states to be forbidden). In detail, TDDFT results show the well known trend, i.e. the B3LYP outcome reaches the best agreement with measurements. The pure BLYP functional produces red-shifted adsorption edges and peak position, while the remaining kernels behaves the other way round, yielding adsorption edges and peak positions at higher energies with respect to experimental measurements. For any tested functional, the decrease of the excitation energies computed from the solution of BSE on top of perturbative GW calculations, causes the theoretical absorption spectra to move to higher wavelengths compared to the TDDFT ones. Therefore the main structures present in the BSE@G₀W₀ spectrum obtained on top of a B3LYP functional are significantly red-shifted with respect to TDDFT, deteriorating the agreement with experiment. To restore a reasonable agreement between theory and experiment it is required to introduce a larger fraction of exact exchange in V_{XC}. However, in the present case the main features of the BHLYP spectrum (similarly to the CAM-B3LYP one) reside at too short wavelengths. On the contrary, the results from a BSE calculation performed on

top of G_nW_n results are almost independent on the underlying choice of V_{xc} , and only small differences can be observed in the position of the main structure of the spectra. Anyway, when compared with experiment, all the tested starting points produces results which slightly underestimate the wavelength of the main structures.

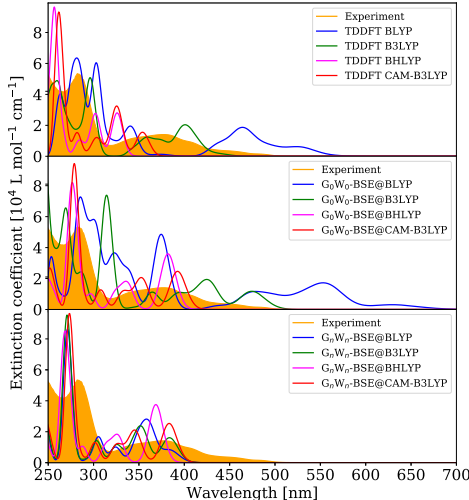


Figure 10: Extinction coefficient of $\text{Ir}(\text{ppy})_3$ obtained at the TDDFT level as well as from the BSE on top on G_0W_0 and G_nW_n results. Calculations have been performed on top on a BLYP, B3LYP, and CAM-B3LYP DFT starting point.

6 Conclusions

We calculated electronic and optical properties of six Ir(III) cyclometalated complexes, widely used as light emitters in OLED devices, using the Many Body Perturbation Theory method GW-BSE, both the one-shot G_0W_0 method, and the eigenvalue self-consistent G_nW_n . The quasiparticle levels (IP and EA) are well described by the ΔSCF and GW method, and the ionization potentials compare reasonably well to available experimental data. The lack of experimental electron affinities does not allow to draw a definite conclusion about the accuracy of the calculated values.

The TDDFT@B3LYP calculated optical absorption spectra are in good agreement with the experimental measurements carried out in this and previous works. Starting from B3LYP wavefunctions, BSE@G₀W₀ results in a red-shift of the spectra, whereas the BSE@G_nW_n results in a blue-shift. We found that by increasing the fraction of Hartree-Fock exchange in the hybrid DFT calculations, the GW eigenvalue self-consistency is less important, and the calculated BSE@G_nW_n absorption spectrum is less dependent from the DFT exchange-correlation, although blue-shifted with respect to experiments.

Our calculations are among the largest GW-BSE calculations reported in the literature^{32,37,42,69,70} and they can provide realistic systems for testing the accuracy of current GW-BSE methods, in order to explore the effects of different self-consistency schemes, and of the underlying DFT exchange-correlation functional.

Supporting Information

The Supporting Information is available free of charge on the ACS Publications website at DOI: 10.1021/acs.jctc.....

Frontier molecular orbitals of the six cyclometalated Ir(III) complexes; single-particle (from DFT calculations) and quasi-particle (from GW calculations) levels; full list of calculated excitation energies, both at the TDDFT and GW-BSE level, with their main orbital transition components.

Acknowledgement

The author thanks Fabien Bruneval for useful suggestions regarding the use of the MolGW code. We acknowledge the CINECA and the Regione Lombardia award under the LISA initiative 2016-2018 (project QUASOLED), for the availability of high performance computing resources and support. This project was partially funded by the GRO program of Samsung Advanced Institute of Technology (SAIT).

References

- (1) Minaev, B.; Baryshnikov, G.; Agren, H. Principles of phosphorescent organic light emitting devices. *Phys. Chem. Chem. Phys.* **2014**, *16*, 1719–1758.
- (2) Tao, Y.; Yuan, K.; Chen, T.; Xu, P.; Li, H.; Chen, R.; Zheng, C.; Zhang, L.; Huang, W. Thermally Activated Delayed Fluorescence Materials Towards the Breakthrough of Organoelectronics. *Adv. Mater.* **2014**, *26*, 7931–7958.
- (3) Baranoff, E.; Curchod, B. F. E. FIrpic: archetypal blue phosphorescent emitter for electroluminescence. *Dalton Trans.* **2015**, *44*, 8318–8329.
- (4) Kesarkar, S.; Mróz, W.; Penconi, M.; Pasini, M.; Destri, S.; Cazzaniga, M.; Ceresoli, D.; Mussini, P. R.; Baldoli, C.; Giovanella, U.; Bossi, A. Near-IR Emitting Iridium(III) Complexes with Heteroaromatic β -Diketonate Ancillary Ligands for Efficient Solution-Processed OLEDs: Structure-Property Correlations. *Angew. Chem. Int. Edit.* *55*, 2714–2718.
- (5) Penconi, M.; Cazzaniga, M.; Kesarkar, S.; Mussini, P. R.; Ceresoli, D.; Bossi, A. Upper limit to the ultimate achievable emission wavelength in near-IR emitting cyclometalated iridium complexes. *Photochem. Photobiol. Sci.* **2017**, *16*, 1220–1229.
- (6) Penconi, M.; Cazzaniga, M.; Kesarkar, S.; Baldoli, C.; Mussini, P. R.; Ceresoli, D.; Bossi, A. β -Diketonate ancillary ligands in heteroleptic iridium complexes: a balance between synthetic advantages and photophysical troubles. *Photochem. Photobiol. Sci.* **2018**, *17*, 1169–1178.
- (7) Gu, X.; Fei, T.; Zhang, H.; Xu, H.; Yang, B.; Ma, Y.; Liu, X. Theoretical Studies of Blue-Emitting Iridium Complexes with Different Ancillary Ligands. *J. Phys. Chem. A* **2008**, *112*, 8387–8393.

- (8) Li, H.; Winget, P.; Risko, C.; Sears, J. S.; Bredas, J.-L. Tuning the electronic and photophysical properties of heteroleptic iridium(III) phosphorescent emitters through ancillary ligand substitution: a theoretical perspective. *Phys. Chem. Chem. Phys.* **2013**, *15*, 6293–6302.
- (9) Iikura, H.; Tsuneda, T.; Yanai, T.; Hirao, K. A long-range correction scheme for generalized-gradient-approximation exchange functionals. *J. Chem. Phys.* **2001**, *115*, 3540–3544.
- (10) Vydrov, O. A.; Scuseria, G. E. Assessment of a long-range corrected hybrid functional. *J. Chem. Phys.* **2006**, *125*, 234109.
- (11) Yanai, T.; Tew, D. P.; Handy, N. C. A new hybrid exchange–correlation functional using the Coulomb-attenuating method (CAM-B3LYP). *Chem. Phys. Lett.* **2004**, *393*, 51–57.
- (12) Jacquemin, D.; Perpète, E. A.; Scuseria, G. E.; Ciofini, I.; Adamo, C. TD-DFT Performance for the Visible Absorption Spectra of Organic Dyes: Conventional versus Long-Range Hybrids. *J. Chem. Theor. Comp.* **2007**, *4*, 123–135.
- (13) Asada, T.; Hamamura, S.; Matsushita, T.; Koseki, S. Theoretical study on the absorption spectra of fac-Ir(ppy)₃ in the amorphous phase of organic electro-luminescent devices. *Res. Chem. Interm.* **2009**, *35*, 851.
- (14) Himmetoglu, B.; Marchenko, A.; Dabo, I.; Cococcioni, M. Role of electronic localization in the phosphorescence of iridium sensitizing dyes. *J. Chem. Phys.* **2012**, *137*, 154309.
- (15) Smith, A. R. G.; Burn, P. L.; Powell, B. J. SpinOrbit Coupling in Phosphorescent Iridium(III) Complexes. *Chem. Phys. Chem.* *12*, 2429–2438.
- (16) Younker, J. M.; Dobbs, K. D. Correlating Experimental Photophysical Properties of

- Iridium(III) Complexes to SpinOrbit Coupled TDDFT Predictions. *J. Phys. Chem. C* **2013**, *117*, 25714–25723.
- (17) Brahim, H.; Daniel, C. Structural and spectroscopic properties of Ir(III) complexes with phenylpyridine ligands: Absorption spectra without and with spinorbit-coupling. *Comp. Theo. Chem.* **2014**, *1040-1041*, 219 – 229.
- (18) Mori, K.; Goumans, T. P. M.; van Lenthe, E.; Wang, F. Predicting phosphorescent lifetimes and zero-field splitting of organometallic complexes with time-dependent density functional theory including spin-orbit coupling. *Phys. Chem. Chem. Phys.* **2014**, *16*, 14523–14530.
- (19) Koseki, S.; Kamata, N.-o.; Asada, T.; Yagi, S.; Nakazumi, H.; Matsushita, T. SpinOrbit Coupling Analyses of the Geometrical Effects on Phosphorescence in Ir(ppy)₃ and Its Derivatives. *J. Phys. Chem. C* **2013**, *117*, 5314–5327.
- (20) Heil, A.; Gollnisch, K.; Kleinschmidt, M.; Marian, C. M. On the photophysics of four heteroleptic iridium(III) phenylpyridyl complexes investigated by relativistic multi-configuration methods. *Mol. Phys.* **2016**, *114*, 407–422.
- (21) Salpeter, E. E.; Bethe, H. A. A Relativistic Equation for Bound-State Problems. *Phys. Rev.* **1951**, *84*, 1232–1242.
- (22) Hedin, L. New Method for Calculating the One-Particle Green’s Function with Application to the Electron-Gas Problem. *Phys. Rev.* **1965**, *139*, A796–A823.
- (23) Hybertsen, M. S.; Louie, S. G. Electron correlation in semiconductors and insulators: Band gaps and quasiparticle energies. *Phys. Rev. B* **1986**, *34*, 5390–5413.
- (24) Onida, G.; Reining, L.; Rubio, A. Electronic excitations: density-functional versus many-body Green’s-function approaches. *Rev. Mod. Phys.* **2002**, *74*, 601–659.

- (25) Martin, R. M.; Reining, L.; Ceperley, D. M. *Interacting Electrons Theory and Computational Approaches*; Cambridge University Press: Cambridge, 2016.
- (26) Reining, L. The GW approximation: content, successes and limitations. *WIRE: Comp. Mol. Sci.* **2017**, *8*, e1344.
- (27) Golze, D.; Dvorak, M.; Rinke, P. The GW Compendium: A Practical Guide to Theoretical Photoemission Spectroscopy. *Front. Chem.* **2019**, *7*, 377.
- (28) Faber, C.; Boulanger, P.; Attaccalite, C.; Duchemin, I.; Blase, X. Excited states properties of organic molecules: from density functional theory to the GW and Bethe-Salpeter Green's function formalisms. *Phil. Trans. R. Soc. Lon. A* **2014**, *372*, 20130271.
- (29) Bruneval, F.; Rangel, T.; Hamed, S. M.; Shao, M.; Yang, C.; Neaton, J. B. molgw 1: Many-body perturbation theory software for atoms, molecules, and clusters. *Comp. Phys. Commun.* **2016**, *208*, 149 – 161.
- (30) Marom, N. Accurate description of the electronic structure of organic semiconductors by GW methods. *J. Phys.: Cond. Mat.* **2017**, *29*, 103003.
- (31) Blase, X.; Duchemin, I.; Jacquemin, D. The Bethe-Salpeter equation in chemistry: relations with TD-DFT, applications and challenges. *Chem. Soc. Rev* **2018**, –.
- (32) Lettmann, T.; Rohlfing, M. Electronic Excitations of Polythiophene within Many-Body Perturbation Theory with and without the Tamm–Dancoff Approximation. *J. Chem. Theor. Comp.* **2019**,
- (33) Blase, X.; Attaccalite, C. Charge-transfer excitations in molecular donor-acceptor complexes within the many-body Bethe-Salpeter approach. *Appl. Phys. Lett.* **2011**, *99*, 171909.
- (34) Ziaei, V.; Bredow, T. GW-BSE approach on S1 vertical transition energy of large charge transfer compounds: A performance assessment. *J. Chem. Phys.* **2016**, *145*, 174305.

- (35) Jacquemin, D.; Duchemin, I.; Blase, X. Is the BetheSalpeter Formalism Accurate for Excitation Energies? Comparisons with TD-DFT, CASPT2, and EOM-CCSD. *J. Phys. Chem. Letters* **2017**, *8*, 1524–1529.
- (36) Bruneval, F.; Marques, M. A. L. Benchmarking the Starting Points of the GW Approximation for Molecules. *J. Chem. Theor. Comp.* **2013**, *9*, 324–329.
- (37) Jacquemin, D.; Duchemin, I.; Blase, X. Benchmarking the BetheSalpeter Formalism on a Standard Organic Molecular Set. *J. Chem. Theor. Comp.* **2015**, *11*, 3290–3304.
- (38) van Setten, M. J.; Caruso, F.; Sharifzadeh, S.; Ren, X.; Scheffler, M.; Liu, F.; Lischner, J.; Lin, L.; Deslippe, J. R.; Louie, S. G.; Yang, C.; Weigend, F.; Neaton, J. B.; Evers, F.; Rinke, P. GW100: Benchmarking G0W0 for Molecular Systems. *J. Chem. Theor. Comp.* **2015**, *11*, 5665–5687.
- (39) Caruso, F.; Dauth, M.; van Setten, M. J.; Rinke, P. Benchmark of GW Approaches for the GW100 Test Set. *J. Chem. Theor. Comp.* **2016**, *12*, 5076–5087.
- (40) Maggio, E.; Liu, P.; van Setten, M. J.; Kresse, G. GW100: A Plane Wave Perspective for Small Molecules. *J. Chem. Theor. Comp.* **2017**, *13*, 635–648.
- (41) Govoni, M.; Galli, G. GW100: Comparison of Methods and Accuracy of Results Obtained with the WEST Code. *J. Chem. Theor. Comp.* **2018**, *14*, 1895–1909.
- (42) Gui, X.; Holzer, C.; Klopper, W. Accuracy Assessment of GW Starting Points for Calculating Molecular Excitation Energies Using the BetheSalpeter Formalism. *J. Chem. Theor. Comp.* **2018**, *14*, 2127–2136.
- (43) Penconi, M.; Cazzaniga, M.; Panzeri, W.; Mele, A.; Cargnoni, F.; Ceresoli, D.; Bossi, A. Unraveling the Degradation Mechanism in FIrpic-Based Blue OLEDs: II. Trap and Detect Molecules at the Interfaces. *Chem. Mater.* **2019**, *31*, 2277–2285.
- (44) Mahan, G. D. *Many particle physics*; Plenum Press: New York, 1981.

- (45) Fetter, A. L.; Walecka, J. D. *Quantum Theory of Many-Particle Physics*; Dover: New York, 2003.
- (46) Hybertsen, M. S.; Louie, S. G. First-Principles Theory of Quasiparticles: Calculation of Band Gaps in Semiconductors and Insulators. *Phys. Rev. Lett.* **1985**, *55*, 1418–1421.
- (47) Godby, R. W.; Schlüter, M.; Sham, L. J. Self-energy operators and exchange-correlation potentials in semiconductors. *Phys. Rev. B* **1988**, *37*, 10159–10175.
- (48) Faleev, S. V.; van Schilfgaarde, M.; Kotani, T. All-Electron Self-Consistent GW Approximation: Application to Si, MnO, and NiO. *Phys. Rev. Lett.* **2004**, *93*, 126406.
- (49) Kotani, T.; van Schilfgaarde, M.; Faleev, S. V. Quasiparticle self-consistent GW method: A basis for the independent-particle approximation. *Phys. Rev. B* **2007**, *76*, 165106.
- (50) CASIDA, M. E. *Recent Advances in Density Functional Methods*; WORLD SCIENTIFIC, 1995; pp 155–192.
- (51) Jacquemin, D.; Duchemin, I.; Blondel, A.; Blase, X. Assessment of the Accuracy of the BetheSalpeter (BSE/GW) Oscillator Strengths. *J. Chem. Theor. Comp.* **2016**, *12*, 3969–3981.
- (52) Rangel, T.; Hamed, S. M.; Bruneval, F.; Neaton, J. B. Evaluating the GW Approximation with CCSD(T) for Charged Excitations Across the Oligoacenes. *J. Chem. Theor. Comp.* **2016**, *12*, 2834–2842.
- (53) Bruneval, F.; Hamed, S. M.; Neaton, J. B. A systematic benchmark of the ab initio Bethe-Salpeter equation approach for low-lying optical excitations of small organic molecules. *J. Chem. Phys.* **2015**, *142*, 244101.
- (54) Frisch, M. J.; Trucks, G. W.; Schlegel, H. B.; Scuseria, G. E.; Robb, M. A.; Cheeseman, J. R.; Scalmani, G.; Barone, V.; Mennucci, B.; Petersson, G. A.; Nakatsuji, H.;

Caricato, M.; Li, X.; Hratchian, H. P.; Izmaylov, A. F.; Bloino, J.; Zheng, G.; Sonnenberg, J. L.; Hada, M.; Ehara, M.; Toyota, K.; Fukuda, R.; Hasegawa, J.; Ishida, M.; Nakajima, T.; Honda, Y.; Kitao, O.; Nakai, H.; Vreven, T.; Montgomery, J. A., Jr.; Peralta, J. E.; Ogliaro, F.; Bearpark, M.; Heyd, J. J.; Brothers, E.; Kudin, K. N.; Staroverov, V. N.; Kobayashi, R.; Normand, J.; Raghavachari, K.; Rendell, A.; Burant, J. C.; Iyengar, S. S.; Tomasi, J.; Cossi, M.; Rega, N.; Millam, J. M.; Klene, M.; Knox, J. E.; Cross, J. B.; Bakken, V.; Adamo, C.; Jaramillo, J.; Gomperts, R.; Stratmann, R. E.; Yazyev, O.; Austin, A. J.; Cammi, R.; Pomelli, C.; Ochterski, J. W.; Martin, R. L.; Morokuma, K.; Zakrzewski, V. G.; Voth, G. A.; Salvador, P.; Dannenberg, J. J.; Dapprich, S.; Daniels, A. D.; Farkas, .; Foresman, J. B.; Ortiz, J. V.; Cioslowski, J.; Fox, D. J. Gaussian09 Revision D.01. Gaussian Inc. Wallingford CT 2013.

(55) <http://www.molgw.org/>.

(56) Dedeian, K.; Djurovich, P. I.; Garces, F. O.; Carlson, G.; Watts, R. J. A new synthetic route to the preparation of a series of strong photoreducing agents: fac-tris-orthometalated complexes of iridium(III) with substituted 2-phenylpyridines. *Inorg. Chem.* **1991**, *30*, 1685–1687.

(57) Lamansky, S.; Djurovich, P.; Murphy, D.; Abdel-Razzaq, F.; Kwong, R.; Tsyba, I.; Bortz, M.; Mui, B.; Bau, R.; Thompson, M. E. Synthesis and Characterization of Phosphorescent Cyclometalated Iridium Complexes. *Inorg. Chem.* **2001**, *40*, 1704–1711.

(58) Tamayo, A. B.; Alleyne, B. D.; Djurovich, P. I.; Lamansky, S.; Tsyba, I.; Ho, N. N.; Bau, R.; Thompson, M. E. Synthesis and Characterization of Facial and Meridional Tris-cyclometalated Iridium(III) Complexes. *J. Amer. Chem. Soc.* **2003**, *125*, 7377–7387.

- (59) McGee, K. A.; Mann, K. R. Selective Low-Temperature Syntheses of Facial and Meridional Tris-cyclometalated Iridium(III) Complexes. *Inorg. Chem.* **2007**, *46*, 7800–7809.
- (60) Li, J.; Zhang, Q.; He, H.; Wang, L.; Zhang, J. Tuning the electronic and phosphorescence properties of blue-emitting iridium(III) complexes through different cyclometalated ligand substituents: a theoretical investigation. *Dalton Trans.* **2015**, *44*, 8577–8589.
- (61) Park, N. G.; Choi, G. C.; Lee, Y. H.; Kim, Y. S. Theoretical studies on the ground and excited states of blue phosphorescent cyclometalated Ir(III) complexes having ancillary ligand. *Curr. Appl. Phys.* **2006**, *6*, 620 – 626.
- (62) Hay, P. J. Theoretical Studies of the Ground and Excited Electronic States in Cyclometalated Phenylpyridine Ir(III) Complexes Using Density Functional Theory. *J. Phys. Chem. A* **2002**, *106*, 1634–1641.
- (63) Park, N. G.; Choi, G. C.; Lee, J. E.; Kim, Y. S. Theoretical studies of cyclometalated phenylpyrazol Ir(III) complex using density functional theory. *Curr. Appl. Phys.* **2005**, *5*, 79 – 84.
- (64) Krbel, S.; Boulanger, P.; Duchemin, I.; Blase, X.; Marques, M. A. L.; Botti, S. Benchmark Many-Body GW and BetheSalpeter Calculations for Small Transition Metal Molecules. *J. Chem. Theor. Comp.* **2014**, *10*, 3934–3943.
- (65) DAndrade, B. W.; Datta, S.; Forrest, S. R.; Djurovich, P.; Polikarpov, E.; Thompson, M. E. Relationship between the ionization and oxidation potentials of molecular organic semiconductors. *Org. Elec.* **2005**, *6*, 11 – 20.
- (66) Yoshida, H.; Yoshizaki, K. Electron affinities of organic materials used for organic light-emitting diodes: A low-energy inverse photoemission study. *Org. Elec.* **2015**, *20*, 24 – 30.

- (67) Smith, A. R.; Burn, P. L.; Powell, B. J. Exact exchange and the density functional theory of metal-to-ligand charge-transfer in fac-Ir(ppy)₃. *Org. Elec.* **2016**, *33*, 110 – 115.
- (68) Jacquemin, D.; Duchemin, I.; Blondel, A.; Blase, X. Benchmark of Bethe-Salpeter for Triplet Excited-States. *J. Chem. Theor. Comp.* **2017**, *13*, 767–783.
- (69) Deslippe, J.; Samsonidze, G.; Strubbe, D. A.; Jain, M.; Cohen, M. L.; Louie, S. G. BerkeleyGW: A massively parallel computer package for the calculation of the quasi-particle and optical properties of materials and nanostructures. *Comp. Phys. Commun.* **2012**, *183*, 1269–1289.
- (70) Govoni, M.; Galli, G. Large Scale GW Calculations. *J. Chem. Theor. Comp.* **2015**, *11*, 2680–2696.

Graphical TOC Entry

